CHEMISTRY OF MATERIALS
Article

Chem. Mater. **2010,** *22,* 1551–1558 1551
DOI:10.1021/cm902970u

Electronic and Structural Properties of $Sn_xTi_{1-x}O_2$ ($0.0 \leq x \leq 0.1$) Solid Solutions

M. Hilni Harunsani, Freddy E. Oropeza, Robert G. Palgrave,* and Russell G. Egdell

Department of Chemistry, Inorganic Chemistry Laboratory, South Parks Road, Oxford OX1 3QR, United Kingdom

Received September 24, 2009. Revised Manuscript Received December 2, 2009

The electronic and structural properties of dilute solid solutions of SnO_2 in TiO_2 have been investigated. Samples of $Sn_xTi_{1-x}O_2$ with $0.0 \leq x \leq 0.1$ (i.e., 0−10% Sn doping) were prepared by solid state reaction of SnO_2 and TiO_2 powders at 1200 °C followed by rapid quenching. Narrowing of the bandgap at low Sn doping level was observed through both diffuse reflectance spectroscopy and valence band photoemission spectroscopy. This provides an explanation of the visible light photocatalytic activity previously reported for this system. X-ray diffraction showed a positive deviation of the lattice parameters from Vegard's Law, whereas Raman spectra revealed a red-shift in the E_g and B_{1g} peaks and a blue-shift in the A_{1g} peak with increasing Sn content.

Introduction

Mixed oxides of rutile TiO_2 and SnO_2 are of interest in the field of gas sensing, where they give enhanced response to H_2 and CO compared to the pure binary oxides,[1−5] and in the field of photocatalysis, where improved activity under UV light[6−13] and visible light[14,15] have been reported, despite the anatase phase of TiO_2 usually being considered more photoactive. In both gas sensing and photocatalysis it has been found that small additions of SnO_2 to TiO_2 give the most beneficial results.[2,9] In both cases the electronic structure of the material is critical to the functional behavior. TiO_2 and SnO_2 both adopt the tetragonal rutile structure, although the lattice parameters for SnO_2 (a = 4.594 Å, c = 2.959 Å) are somewhat bigger than those for TiO_2 (a = 4.737 Å, c = 3.360 Å). Substitutional solid solutions $Sn_xTi_{1-x}O_2$ which retain the rutile structure of the end members are obtained by reaction between SnO_2 and TiO_2 at elevated temperatures.[2,16,17] Above 1450 °C solid solutions across the complete composition range $0.0 < x < 1.0$ are thermodynamically stable.[18] Below 1450 °C there is a roughly symmetrical miscibility gap, within which solid solution undergo spinodal decomposition into Sn and Ti rich phases.[19−21] However, such decomposition is slow at room temperature, and rapid quenching of compositions close to the end members ($x < 0.2$, $x > 0.8$) gives single phase samples which are stable for long periods;[17,22,23] alternatively, metastable compositions can be made close to room temperature under kinetic control.[24]

While the individual electronic structures of TiO_2 and SnO_2 have been well studied over many years,[25−30] the

*Author to whom correspondence should be addressed.

(1) Zakrzewska, K. *Thin Solid Films* **2001**, *391*, 229–238.
(2) Radecka, M.; Zakrzewska, K.; Rekas, M. *Sens. Actuators, B* **1998**, *47*, 194–204.
(3) Carney, C. M.; Yoo, S.; Akbar, S. A. In *10th International Meeting on Chemical Sensors*; Elsevier Science Sa: Tsukuba, Japan, 2004; p 29−33.
(4) Tai, W. P.; Oh, J. H. *Sens. Actuators, B* **2002**, *85*, 154–157.
(5) Carotta, M. C.; Gherardi, S.; Guidi, V.; Malagu, C.; Martinelli, G.; Vendemiati, B.; Sacerdoti, M.; Ghiotti, G.; Morandi, S.; Bismuto, A.; Maddalena, P.; Setaro, A. *Sens. Actuators, B* **2008**, *130*, 38–45.
(6) Cai, Z. Q.; Shen, Q. H.; Gao, J. W.; Yang, H. *J. Inorg. Mater.* **2007**, *22*, 733–736.
(7) Fresno, F.; Guillard, C.; Coronado, J. M.; Chovelon, J. M.; Tudela, D.; Soria, J.; Herrmann, J. M. *J. Photochem. Photobiol., A* **2005**, *173*, 13–20.
(8) Fresno, F.; Coronado, J. A.; Tudela, D.; Soria, J. *Appl. Catal., B* **2005**, *55*, 159–167.
(9) Lin, J.; Yu, J. C.; Lo, D.; Lam, S. K. *J. Catal.* **1999**, *183*, 368–372.
(10) Jing, L. Q.; Fu, H. G.; Wang, D. J.; Wei, X.; Sun, J. Z. *Acta Phys. -Chim. Sin.* **2005**, *21*, 378–382.
(11) Cao, Y. A.; Yang, W. S.; Zhang, W. F.; Liu, G. Z.; Yue, P. L. *New J. Chem.* **2004**, *28*, 218–222.
(12) Lin, C. F.; Wu, C. H.; Onn, Z. N. *J. Hazard. Mater.* **2008**, *154*, 1033–1039.
(13) Tada, H.; Hattori, A.; Tokihisa, Y.; Imai, K.; Tohge, N.; Ito, S. *J. Phys. Chem. B* **2000**, *104*, 4585–4587.
(14) Sayilkan, F.; Asiltuerk, M.; Tatar, P.; Kiraz, N.; Sener, S.; Arpac, E.; Sayilkan, H. *Mater. Res. Bull.* **2008**, *43*, 127–134.
(15) Kutty, T. R. N.; Avudaithai, M. *Chem. Phys. Lett.* **1989**, *163*, 93–97.
(16) Sinclair, W. R.; Loomis, T. C. *Angew. Chem., Int. Ed.* **1958**, *70*, 603–603.
(17) Drobeck, D. L.; Virkar, A. V.; Cohen, R. M. *J. Phys. Chem. Solids* **1990**, *51*, 977–988.
(18) Naidu, H. P.; Virkar, A. V. *J. Am. Ceram. Soc.* **1998**, *81*, 2176–2180.
(19) Nambu, S.; Oiji, M. *J. Am. Ceram. Soc.* **1991**, *74*, 1910–1915.
(20) Cohen, R. M.; Drobeck, D.; Virkar, A. V. *J. Am. Ceram. Soc.* **1988**, *71*, C401–C403.
(21) Kong, L. B.; Ma, J.; Huang, H. *J. Alloys Compd.* **2002**, *336*, 315–319.
(22) Hirata, T.; Ishioka, K.; Kitajima, M.; Doi, H. *Phys. Rev. B* **1996**, *53*, 8442–8448.
(23) Kulshreshtha, S. K.; Sasikala, R.; Sudarsan, V. *J. Mater. Chem.* **2001**, *11*, 930–935.
(24) Uchiyama, H.; Imai, H. *Chem. Commun.* **2005**, 6014–6016.
(25) Robertson, J. *Phys. Rev. B* **1984**, *30*, 3520–3522.
(26) Mazzone, A. M. *Philos. Mag. Lett.* **2004**, *84*, 275–282.
(27) Freeman, C. M.; Catlow, C. R. A. *J. Solid State Chem.* **1990**, *85*, 65–75.
(28) Cox, D. F.; Fryberger, T. B.; Semancik, S. *Phys. Rev. B* **1988**, *38*, 2072–2083.
(29) Batzill, M.; Diebold, U. *Prog. Surf. Sci.* **2005**, *79*, 47–154.
(30) Glassford, K. M.; Chelikowsky, J. R. *Phys. Rev. B* **1992**, *46*, 1284–1298.

Published on Web 01/05/2010

electronic structures of $Sn_xTi_{1-x}O_2$ solid solutions have been investigated only recently, and chiefly by theoretical means.[31−33] Rutile TiO_2 and SnO_2 both have direct bandgaps of magnitude 3.062 and 3.596 eV, respectively.[34−36] In SnO_2 the valence and conduction bands are both offset to lower energies in comparison with TiO_2. Thus when TiO_2 and SnO_2 are bought together in a heterojunction, photoexcited electrons from TiO_2 are transferred across the interface to the SnO_2 phase with no applied voltage.[13,37,38] This suggests that the SnO_2 conduction band minimum is lower in energy than TiO_2, a conjecture corroborated by theoretical calculations.[39]

Sensato et al. performed periodic density functional theory (DFT) calculations on rutile $Sn_xTi_{1-x}O_2$ and predicted a monotonic increase of the direct band gap with increasing Sn content, but also the presence of a lower energy (2.9 eV) indirect band gap present at low Sn concentrations.[31] Taft et al. performed DFT calculations on Sn doped TiO_2 (110) surfaces, and found the nature and magnitude of the band gap to be highly dependent on the location of the substitutional Sn cation.[32] For most substitutional sites, the direct bandgap of TiO_2 was found to increase with the addition of Sn, but one site was found where an indirect gap smaller than that of the undoped surface arose as a consequence of Sn doping. Long et al., also using DFT, found a decrease in the band gap of rutile TiO_2 upon Sn doping caused by the lowering of the conduction band energy.[33] Higher levels of Sn doping were, however, found to cause an increase in the band gap. While these theoretical studies are interesting, there has been little detailed experimental work of the electronic structure of $Sn_xTi_{1-x}O_2$.

In this paper we report a study of $Sn_xTi_{1-x}O_2$ solid solutions in the composition range $0.0 \leq x \leq 0.10$. The magnitude of the optical bandgap, which is important for photocatalysis applications, was determined through diffuse reflectance (DR) spectroscopy and changes in the valence band were measured using high resolution X-ray photoelectron spectroscopy (XPS). Structural changes were investigated using X-ray diffraction and Raman spectroscopy.

Experimental Section

Rutile TiO_2 (Aldrich, 99.9%) and SnO_2 (Aldrich, 99.9%) powders were weighed in the desired ratio and ground together in an agate mortar. The resulting mixture was placed in recrystallized alumina boats and heated to 1200 °C in air for 3−6 days. To avoid the spinodal decomposition that can occur during slow cooling, the samples were quenched by removal from the furnace at 1200 °C into air, followed by cooling on the benchtop. Powder X-ray diffraction (XRD), carried out on a Panalytical X'Pert Pro instrument using monochromated Cu $K\alpha_1$ radiation, was used to assess phase purity. Samples found to be multiphase were reground and refired at 1200 °C until a single phase was obtained. High resolution X-ray photoemission spectra (XPS) were recorded on a Scienta ESCA 300 spectrometer located at Daresbury Laboratory, UK, which incorporated a rotating anode Al Kα ($h\nu$ = 1486.6 eV) X-ray source. The X-ray source was run with 200 mA emission current and 14 kV anode bias, while the analyzer operated at 150 eV pass energy with 0.8 mm slits. Gaussian convolution of the analyzer resolution with a line width of 260 meV for the monochromated X-ray source gives an effective instrument resolution of 400 meV. The spectrometer was calibrated regularly to set the Fermi edge of a silver reference sample at zero binding energy. Powder samples of Sn-doped TiO_2 were prepared for XPS analysis by pressing into indium foil. Extra care was taken to ensure that the coverage of the indium foil was complete and that no In peaks appeared in the photoelectron spectra. A weak C 1s peak was evident in most spectra with a C 1s to O 1s intensity ratio typically around 0.03. After correction for atomic sensitivity factors this corresponds to a surface C/O ratio of about 0.08. Given that around 10% of the signal in Al Kα XPS derives from the topmost atomic layer this corresponds to just under 1 monolayer of surface hydrocarbon contamination. Fortunately the ionization cross sections at $h\nu$ = 1486.6 eV for C 2p (5 barns) and H 1s (0.2 barns) states are much lower than those for O 2p (60 barns) or Ti 3d (85 barns) states, so that the contamination layer will contribute around only 1% of the intensity in valence band photoemission spectra. For most samples it was necessary to use an electron flood gun to stabilize the surface charge. Use of a flood gun shifts all spectral features to high kinetic energy. Photoelectron spectra were therefore charge calibrated using the weak C 1s contaminant peak which was assigned a binding energy of 285.0 eV. It was confirmed that this calibration procedure places the Fermi level of metallic thin film samples on highly insulating substrates (e.g., degenerately Sn-doped In_2O_3 on zirconia substrates) at zero binding energy. Thus we may be confident that the binding energies in all our spectra are relative to the Fermi level of the sample. Diffuse reflectance (DR) spectra were measured in the visible and near-ultraviolet (UV) region using a Perkin-Elmer Lambda 750S instrument incorporating a 60 cm integrating sphere. Raman spectra were recorded at room temperature using a Perkin-Elmer RamanStation 400F spectrometer with excitation by a He/Ne laser.

Results and Discussion

X-ray Diffraction. Figure 1 shows X-ray diffraction patterns of the $Sn_xTi_{1-x}O_2$ solid solution over the range of concentrations studied. A clean set of diffraction peaks characteristic of a single rutile phase was observed for all samples. A shift of the diffraction peaks toward lower 2θ angles with increasing Sn content was observed, which is a consequence of the expansion of the TiO_2 unit cell due to substitutional incorporation of Sn onto Ti sites.[9,22,40]

From the positions of the diffraction peaks, the tetragonal lattice parameters a and c were calculated using a

(31) Sensato, F. R.; Custodio, R.; Longo, E.; Beltran, A.; Andres, J. *Catal. Today* **2003**, *85*, 145–152.
(32) Sambrano, J. R.; Nobrega, G. F.; Taft, C. A.; Andres, J.; Beltran, A. *Surf. Sci.* **2005**, *580*, 71–79.
(33) Long, R.; Dai, Y.; Huang, B. *J. Phys. Chem. C* **2009**, *113*, 650–653.
(34) Robertson, J. *J. Phys. C: Solid State Phys.* **1979**, *12*, 4767–4776.
(35) Mo, S. D.; Ching, W. Y. *Phys. Rev. B* **1995**, *51*, 13023–13032.
(36) Maki-Jaskari, M. A.; Rantala, T. T. Phys. Rev. B: Condens. Matter Mater. Phys. **2001**, *64*, no.-075407.
(37) Vinodgopal, K.; Kamat, P. V. *Environ. Sci. Technol.* **1995**, *29*, 841–845.
(38) Zhou, M. H.; Yu, J. G.; Liu, S. W.; Zhai, P. C.; Jiang, L. *J. Hazard. Mater.* **2008**, *154*, 1141–1148.
(39) Beltran, A.; Andres, J.; Sambrano, J. R.; Longo, E. *J. Phys. Chem. A* **2008**, *112*, 8943–8952.
(40) Uchiyama, H.; Imai, H. *Chem. Commun.* **2005**, 6014–6016.

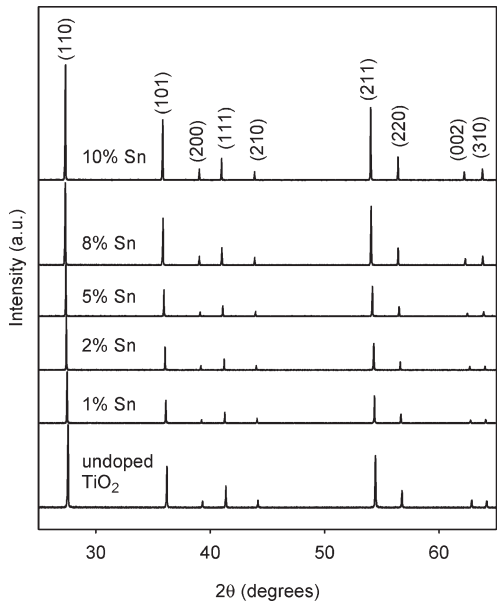

Figure 1. X-ray diffraction patterns (Cu $K\alpha_1$) for $Sn_xTi_{1-x}O_2$ solid solutions of the compositions indicated produced by high temperature solid state reaction. A single set of rutile peaks is observed in each case.

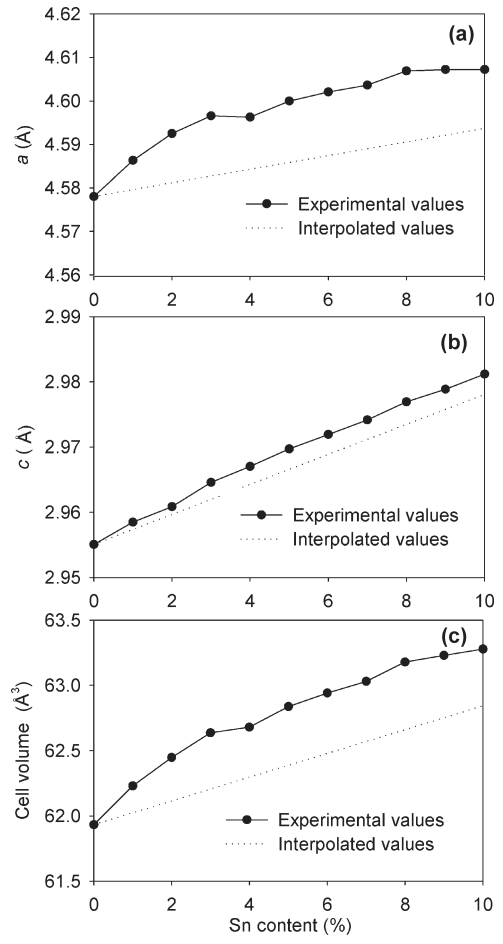

Figure 2. Experimentally determined lattice parameters and cell volume of $Sn_xTi_{1-x}O_2$ solid solutions with 0 − 10% Sn content. Dotted lines show linearly interpolated values linking the TiO_2 and SnO_2 end members (Vegard's Law).

least-squares fit to all reflections in the range $20° < 2\theta < 70°$. In Figure 2, the values of a and c are plotted as a function of x for $Sn_xTi_{1-x}O_2$. The unit cell volumes $V = a^2c$ are also presented. It can be clearly seen that both lattice parameters and the unit cell volumes of the solid solutions increase with x, indicating expansion of the lattice. However, the increase of the a and c values is not linear with Sn concentration and in general the values lie above that expected by linear interpolation between limiting values for TiO_2 and SnO_2. Deviations from Vegard's law have been reported before for this system.[22,31,41] Although deviation from Vegard's law is frequently accompanied by phase separation caused by spinodal decomposition,[31] the phase purity of the samples found by XRD analysis suggests this decomposition not to be the cause of the deviation. In their theoretical work, Sensato et al. found marked deviations from the Vegard's law for phase pure $Sn_xTi_{1-x}O_2$ solid solutions,[31] in agreement with the present experimental results. As shown in Figure 2 the deviation found for the a lattice parameter was greater than that found for the c parameter. This result can be related to the anisotropy in compressibility (κ) for the rutile TiO_2, being $\kappa_a = 1.93 \times 10^{-4}\,kbar^{-1}$ along the a axis and $\kappa_c = 0.87 \times 10^{-4}\,kbar^{-1}$ along the c axis.[42] These values indicate that in TiO_2 the displacement of ions in the $\langle 100 \rangle$ direction is larger than the displacement in the $\langle 001 \rangle$ direction when external forces are applied to a crystal. Therefore, the larger deviation of the a parameter may be a result of a more effective relaxation of stress brought about by incorporation of the larger Sn cations onto Ti sites in the $\langle 100 \rangle$ directions than in the [001] direction. However this analysis will only be valid for low Sn concentrations because in SnO_2, the anisotropy of the compressibilities is reversed in comparison to TiO_2. In SnO_2 $\kappa_c > \kappa_a$,[42] and in studies of the whole range of compositions for $Sn_xTi_{1-x}O_2$ solid solutions, the variations in a and c lattice parameters are found to be complex.[22,31]

Raman Spectroscopy. Rutile TiO_2 and SnO_2 belong to the space group D_{4h} ($P4_2/mnm$) and display four Raman active fundamental vibrational modes, $A_{1g} + B_{1g} + B_{2g} + E_g$.[43] Raman spectra taken on the undoped TiO_2 sample showed peaks at 143 cm^{-1}, 447 cm^{-1} and 610 cm^{-1} which are assigned in accordance with the literature to the B_{1g}, E_g, and A_{1g} vibrations respectively (Figure 3).

The broad feature around 235 cm^{-1} is a combination band,[43,44] and the B_{2g} vibration, expected at 826 cm^{-1} is not observed due to its weak intensity.[22] Sn doping did not cause the appearance of any additional bands, but increasing Sn doping has differing effects on the frequencies of the fundamental vibrations. The B_{1g} and the E_g vibrations show a general shift to lower frequencies with increasing Sn doping, while the opposite trend is seen in the A_{1g} vibration, that is, there is a shift to *higher*

(41) Park, M.; Mitchell, T. E.; Heuer, A. H. *J. Am. Ceram. Soc.* **1975**, *58*, 43–47.
(42) Peercy, P. S.; Morosin, B. *Phys. Rev. B* **1973**, *7*, 2779–2786.
(43) Porto, S. P. S.; Fleury, P. A.; Damen, T. C. *Phys. Rev.* **1967**, *154*, 522–&.
(44) Ma, H. L.; Yang, J. Y.; Dai, Y.; Zhang, Y. B.; Lu, B.; Ma, G. H. *Appl. Surf. Sci.* **2007**, *253*, 7497–7500.

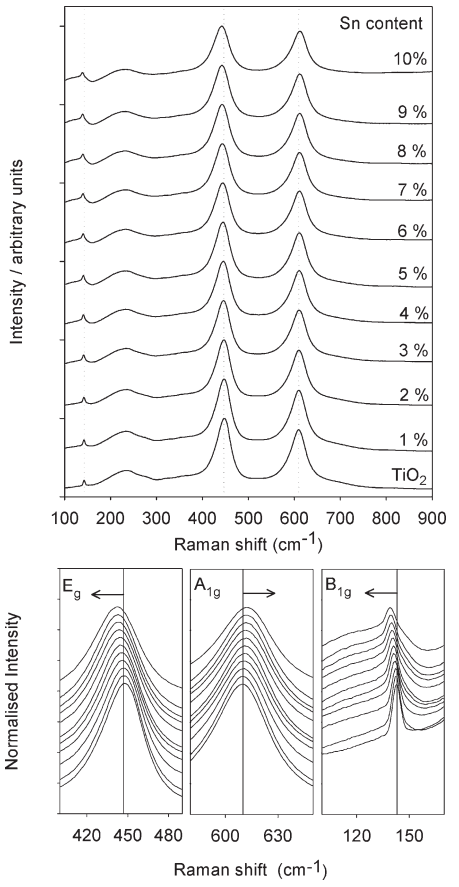

Figure 3. Raman spectra of $Sn_xTi_{1-x}O_2$ solid solutions with 0−10% Sn content. Dotted vertical lines show the positions of TiO_2 Raman peaks. Bottom, expanded views of the E_g, A_{1g}, and B_{1g} Raman peaks. The solid vertical line shows the TiO_2 peak position and the arrow indicates the change caused by increasing Sn doping.

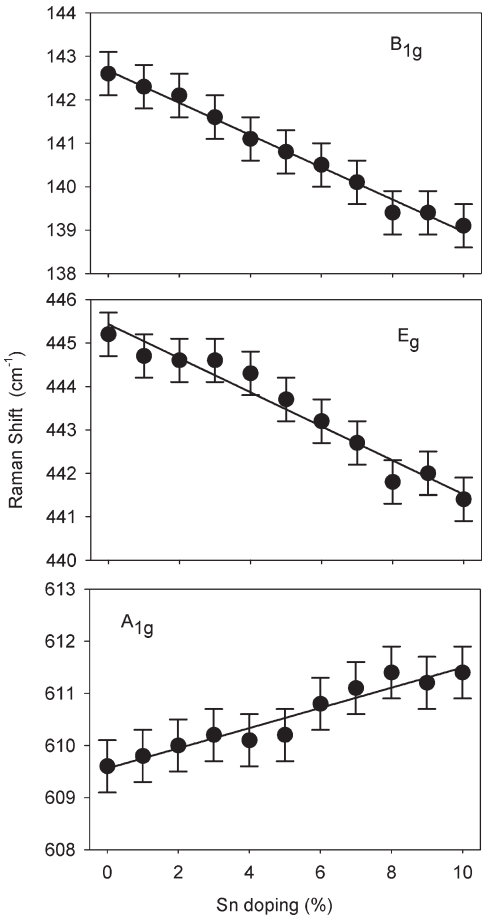

Figure 4. Peak positions of the B_{1g}, E_g, and A_{1g} bands in Raman spectra of $Sn_xTi_{1-x}O_2$ solid solutions with changing Sn content.

frequencies. In each case, the change in frequency is close to linear with Sn concentration (Figure 4).

The frequency of vibrational modes can be affected by particle size for nanoscale crystals. However, since there is no significant variation in crystallite size in the current samples as determined from the full width at half-maximum height (fwhm) of the diffraction peaks, this effect cannot explain the variations in Raman shifts seen here. In SnO_2 (TiO_2), the B_{1g}, E_g, and A_{1g} vibrations appear at 123 (143) cm^{-1}, 475 (447) cm^{-1} and 634 (610) cm^{-1} respectively. Thus, while dilute doping of TiO_2 with Sn causes the A_{1g} and B_{1g} to vibrations shift *toward* their values in SnO_2, the E_g vibration shifts *away* from its value in SnO_2 value. Hirata et al. studied the Raman spectra of $Sn_xTi_{1-x}O_2$ solid solutions across the whole composition range and found the frequency of the E_g fundamental vibrational mode to vary in a nonmonotonic fashion as a function of x, but with behavior similar to that found here at low doping levels.[22] They also found an increase in the frequency of the A_{1g} mode at low doping levels but did not report on variations for the B_{1g} mode. The qualitatively different ways in which the E_g frequency on the one hand and the A_{1g} and B_{1g} frequencies on the other vary with doping in relation to the changes between the end members TiO_2 and SnO_2 may be linked to the fact that atomic displacements for E_g are parallel to the c axis, whereas for A_{1g} and B_{1g}, the displacements are perpendicular to the c axis. Nonetheless as noted by Hirata et al. it is puzzling that the frequencies for both the B_{1g} and E_g modes are higher in SnO_2 than in TiO_2 even though the metal oxygen bonds are shorter in the latter oxide.

Optical Band Gap. The UV−visible absorption spectrum of a semiconductor contains information on its band gap. TiO_2 has a strong and broad absorption feature in the UV region due to inter band electronic transitions.[40,45,46] The variation in absorption coefficient (α) as a function of photon energy ($h\nu$) close to a band edge can typically be fitted to a power law relationship of the following sort:

$$h\nu\alpha(\nu) = B(h\nu - \Delta_g)^n \qquad (1)$$

where B is a constant, Δ_g is the band gap energy, and n takes on a value that depends on the nature of the transition at the bandedge. Values of $n = {}^1/_2$ and $n = 2$ result in a linear fit for direct and indirect transitions respectively.[47] This approach has been extensively used in the study of optical properties of many type of samples, for example, TiO_2 thin films[45] and powders, CdS thin films,[48], and SnO_2

(45) Mahanty, S.; Roy, S.; Sen, S. *J. Cryst. Growth* **2004**, *261*, 77–81.
(46) Du, P.; Moulijn, J. A.; Mul, G. *J. Catal.* **2006**, *238*, 342–352.
(47) Smith, R. A. *Semiconductors*; 2nd ed.; Cambridge University Press: Cambridge, 1978.
(48) Biswas, S.; Hossain, M. F.; Takahashi, T.; Kubota, Y.; Fujishima, A. *Thin Solid Films* **2008**, *516*, 7313–7317.

thin films and nanopowders.[49] Optical transmission in the bulk powder samples studied in this work is very low, and hence the absorption coefficient could not be directly measured. However, the diffuse reflectance spectrum of a sample also contains information on the absorption of the material.[50] The Kubelka−Munk remission function $F(R)$ relates the reflectivity R of a sample to an absorption coefficient α and a scattering coefficient s as follows:

$$F(R) = (1-R)^2/2R = \alpha/s \qquad (2)$$

Assuming a constant scattering coefficient s, $F(R)$ is seen to be proportional to α and thus to represent the absorbance of the sample.[51] This assumption is commonly made in the study of optical properties of powdered materials.[49,52]

From the UV−visible diffuse reflectance data, the absorption spectra of the samples were calculated by means of the Kubelka−Munk function (eq 2). Figure 5 shows the absorption spectra of selected samples in the range of concentration studied. The spectra of all samples show the characteristic broad absorption band that TiO_2 presents due to its fundamental band gap transition. A close examination of the band absorption in the spectra of the samples shows that the spectral edges of the doped samples are shifted toward higher wavelength compared with the undoped TiO_2.

The band gap of the samples was calculated by fitting the absorption band edge of the spectra to eq 1. As $F(R)$ is proportional to α, it can be seen that the linear portion of a plot $[F(R)\,h\nu]^{1/n}$ versus $h\nu$ intercepts the abscissa at $h\nu = \Delta_g$, and this type of plot is commonly used in the estimation of the band gap energy of semiconductors.[45,49,52] Since the fundamental interband electronic transition for both TiO_2 and SnO_2 is direct, a value of $n = {}^1/_2$, that is, the model for direct band gap transitions was used, and good linear fits were obtained as shown in Figure 5(c). Figure 5(d) and 5(e) show values of band gap as a function of Sn concentration for all the samples studied in the present work. It can be seen that the band gap decreases with increasing Sn content at low doping levels and reaches a minimum for 2% Sn doped TiO_2. At higher Sn doping levels the band gap increases monotonically with increasing Sn doping although it does not converge onto the value obtained by linear interpolation between the limits for TiO_2 and SnO_2 within the range of compositions investigated. Thus it appears that negative band bowing occurs in the $Sn_xTi_{1-x}O_2$ system at low doping levels. It should be noted that some experimental and theoretical studies have found a monotonic increase of the band gap as the Sn concentration increases.[31,53] However these earlier investigations involved the complete

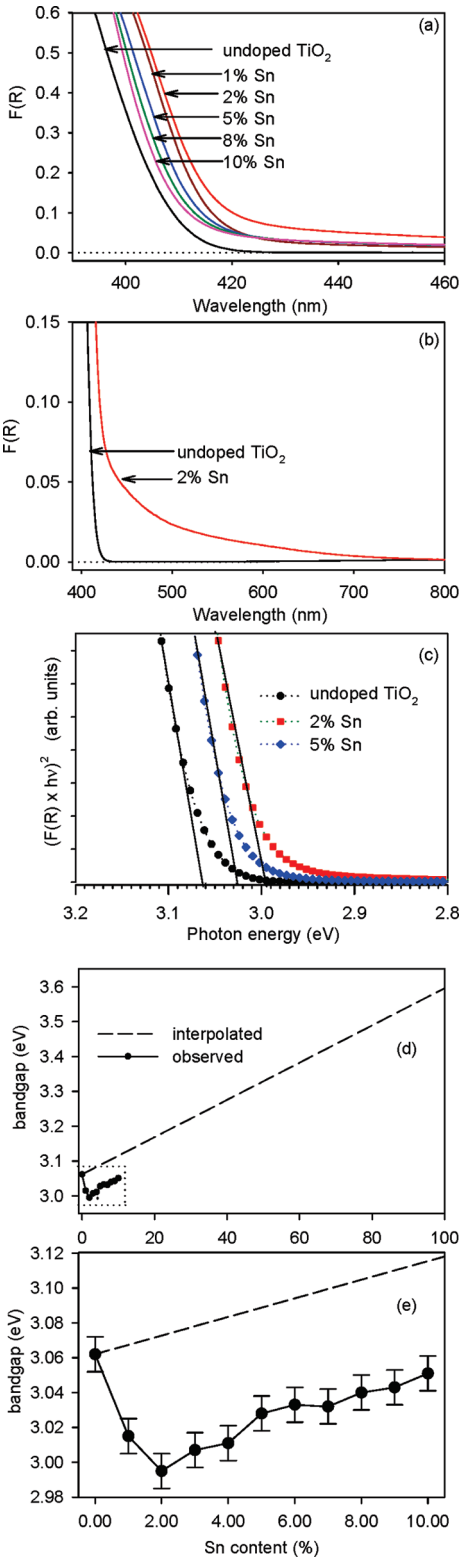

Figure 5. (a) Kubelka−Munk remission function $F(R)$ derived from diffuse reflectance spectra, for several representative samples of $Sn_xTi_{1-x}O_2$ of the compositions indicated close to the band edge. The shift in band edge with doping is apparent. (b) Comparison of $F(R)$ for undoped and 2% Sn doped TiO_2 over the visible region, showing a pronounced tail into the visible region in the doped sample. (c) Band gap plots of $(F(R)h\nu)^2$ for several representative samples, showing extrapolation of the straight line portion to determine the direct band gap. (d) and (e) Variation in optical band gap of $Sn_xTi_{1-x}O_2$ with varying Sn concentration. Dashed line is a linear interpolation between the band gap values for TiO_2 (3.062 eV) and SnO_2 (3.596 eV). Negative band bowing is apparent.

(49) Deng, H. M.; Hossenlopp, J. M. *J. Phys. Chem. B* **2005**, *109*, 66–73.
(50) Cox, P. A. *Electronic Structure and Chemistry of Solids*; Oxford University Press: Oxford, 1987.
(51) Ranga Rao, G.; Ranja Sahu, H. *Proc. Indian Acad. Sci.* (*Chem. Sci.*) **2001**, *113*, 651.
(52) Pang, G. S.; Chen, S. G.; Koltypin, Y.; Zaban, A.; Feng, S. H.; Gedanken, A. *Nano Lett.* **2001**, *1*, 723–726.
(53) Zakrzewska, K.; Radecka, M.; Rekas, M. *Thin Solid Films* **1997**, *310*, 161–166.

composition range with broad steps of $x = 0.1$ between different samples. Thus the behavior at very low doping levels was not identified. In more recent theoretical work, Long et al.[33] found a band gap reduction of 0.12 eV when one Sn is substituted for Ti in a rutile $2 \times 2 \times 2$ supercell (i.e., 1 Ti in every 16) to give a material with 6.25% Sn doping. The band gap increases by 0.06 eV from this reduced value when the doping level is increased to 12.5% (corresponding to one Sn atom in a $2 \times 2 \times 1$ supercell) although there still an overall reduction in the bandgap of 0.06 eV at this doping level as compared to undoped TiO_2. Qualitatively at least these theoretical results mirror our present experimental findings.

It is important to note that as well as leading to a shift in the band edge, Sn doping leads to a very broad but quite weak tail of absorption that extends across much of the visible region down to around 700 nm (corresponding to an energy of 1.7 eV), as shown in Figure 5(b). As discussed below this extra structure is tentatively assigned to reduced Sn^{2+} cations occupying sites at surfaces or grain boundary interfaces.

X-ray Photoelectron Spectroscopy. The reduction of the band gap of $Sn_xTi_{1-x}O_2$ at low Sn concentrations observed by optical spectroscopy can be caused either by an increase in energy of the valence band maximum (VBM) or a decrease in energy of the conduction band minimum (CBM), or both effects simultaneously. XPS is able to test these possibilities through measurement of the filled valence band states, and it may be determined whether filled states exist in doped samples above the VBM of undoped TiO_2. Here the peaks in the valence band spectrum serve as an internal reference from which it is possible to gauge if the valence band edge has moved up in energy. The second possibility can be tested through measurement of the shift in core spectral lines that would be caused by a lowering of the CBM. In *n*-type semiconductors, the Fermi level is pinned near to the CBM by donor states. Thus a reduction in energy of the CBM will lead to a reduction in energy of the Fermi level and a consequent shift of all structure in the photoelectron spectrum (including the core lines) to low binding energy. In practice there are several caveats to this use of XPS to investigate valence band structure and Fermi level position. The short mean free path of electrons within a solid means that Al Kα XPS necessarily measures surface rather than bulk electronic structure. At the surface, the valence band and conduction band are likely to be offset (bent) away from their bulk positions by surface electronic states, and correspondingly, the Fermi level at the surface may be different to that in the bulk. Second, filled surface states within the band gap may be present in photoemission spectra which do not reflect the bulk electronic structure. Finally binding energies in XPS are affected by both initial and final state effects.

Valence band and shallow core level photoelectron spectra of TiO_2 and several Sn-doped TiO_2 samples are shown in Figure 6. For comparison, the intensity in each spectrum in Figure 6 has been normalized to the O 2s peak which appears at a binding energy of 22.2 eV, with less

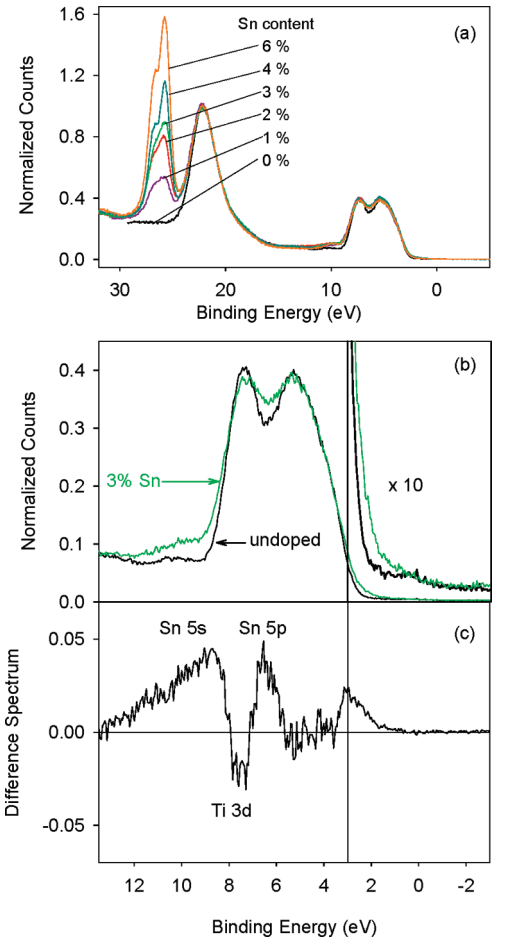

Figure 6. (a) Valence band photoelectron spectra of TiO_2 and $Sn_xTi_{1-x}O_2$ solid solutions (Sn concentrations 1, 2, 3, 4, and 6%) encompassing O 2p bands, the O 2s band and shallow core Sn 4d levels. Spectral intensities are normalized relative to the O 2s core line at 22.2 eV. (b) Detail of the O 2p valence bands of TiO_2 and 3% $Sn_xTi_{1-x}O_2$. The vertical line at 3.06 eV denotes the bandgap of *un*doped rutile TiO_2. (c) Difference spectrum (3% Sn doped−undoped) showing changes due to Sn doping. Labels refer to contributions of metal orbitals to the total density of states.

than 0.1 eV variation in energy between samples. The most readily identified change in the spectra on addition of Sn is the emergence of a doublet whose principle component lies at a binding energy of 25.7 eV, with a splitting of 0.7 eV. This peak increases in intensity with increasing Sn content and is assigned as the Sn 4d shallow core line.[54] The valence band itself straddles binding energies between 3.0 and 12.0 eV and is shown in detail for undoped TiO_2 and 3% Sn doped TiO_2 in Figure 6. Our experimental spectra are referenced to the Fermi level, which is pinned to the bottom of the conduction band in *n*-type semiconductors such as TiO_2 and SnO_2.[55] Sn derived states in the valence band of $Sn_xTi_{1-x}O_2$ with small values of x will appear at lower binding energies relative to the Fermi level than they do in SnO_2, since SnO_2 has a significantly larger band gap (3.60 eV) than TiO_2 (3.06 eV). Therefore in order to compare Sn-induced

(54) Themlin, J. M.; Chtaib, M.; Henrard, L.; Lambin, P.; Darville, J.; Gilles, J. M. *Phys. Rev. B* **1992**, *46*, 2460–2466.
(55) Egdell, R. G.; Eriksen, S.; Flavell, W. R. *Solid State Commun.* **1986**, *60*, 835–838.

features in the current spectra with valence band spectra of SnO_2 it is necessary to take account of a shift to low binding energy of about 0.5 eV. Despite significant covalency in both TiO_2 and SnO_2 bandstructure calculations show that the valence bands in both TiO_2 and SnO_2 are composed primarily of O 2p states with smaller contributions from the metal cations.[35,56] As a consequence, the valence band shows only small changes upon substituting Sn onto Ti sites within the doping range investigated in this study, and these changes are best illustrated in the difference spectra as shown in Figure 6. Each Sn doped sample showed very similar changes in this region, and so for clarity, in Figure 6 only spectra from undoped TiO_2 and 3% Sn doped TiO_2 are shown. Upon Sn doping, there is an increase in spectral weight between binding energies of 8.0−11.5 eV, with the greatest increase at a binding energy of 8.5 eV. There is also a separate sharp increase in spectral weight centered at a binding energy of 6.5 eV. After inclusion of the 0.5 eV correction, these two energies correspond to the regions of the valence band of SnO_2 where there is pronounced hybridization of Sn 5s and Sn 5p states, respectively, with O 2p states.[56] The broad feature with maximum at 8.5 eV is therefore assigned to hybridized Sn 5s−O 2p states, whereas the sharper feature at 6.5 eV is assigned to hybridized Sn 5p−O 2p states. Both Long et al. and Sensato et al. in their respective DFT studies of bulk $Sn_xTi_{1-x}O_2$ predicted contributions from Sn to the valence band states at energies close to those found in the present work.[31,33] We also observe a decrease in spectral weight upon Sn doping at a binding energy of 7.5 eV. This binding energy corresponds to the region of valence band of TiO_2 where there is a maximum contribution from Ti 3*d* states.[35] Therefore the changes in the valence band can be linked with the introduction of Sn derived states and the removal of Ti derived states that would occur upon substitutional doping of Sn for Ti. As expected from the calculations the top of the valence band spectra from 5.5 to 4.0 eV shows almost no change upon Sn doping, as this region is composed almost entirely of O 2p derived states and has close to zero contribution from the metal cations. However, there is another significant change in the valence band spectra: an increase in spectral weight above the VBM of TiO_2 upon Sn doping, which can clearly be seen in the difference spectrum in Figure 6. The changes involve a very small upward shift in the main valence band edge relative to the peak in the valence band spectrum at around 5 eV in addition to the appearance of weak but well-defined structure which straddles the lower half of the valence band. Each Sn doped sample showed an increase in these effects, and the difference spectra for several samples between binding energies of 3.0−0.0 eV binding energy are shown in Figure 7(a).

It can be seen that the integrated area of structure above the VBM of TiO_2 a (taken as 3.0 eV) increases from 0 to 4% Sn doping and then falls from 4 to 6% Sn doping. The increase is dominated not by the small shift in the position

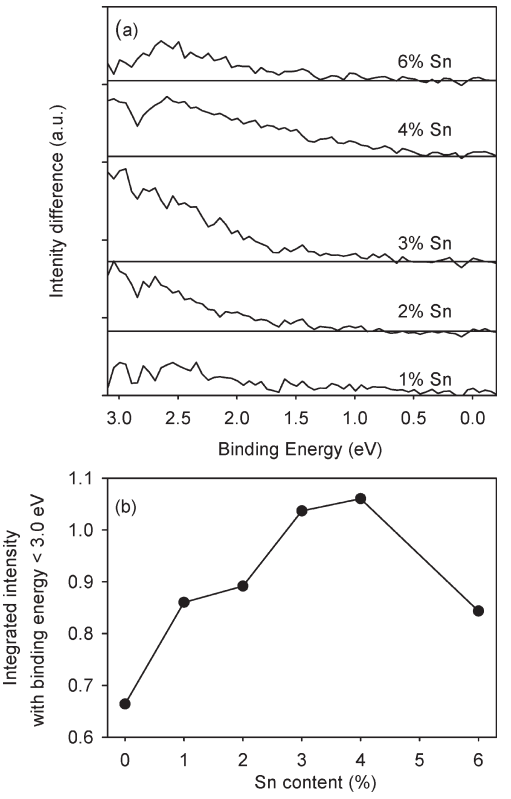

Figure 7. (a) Difference spectra (Sn doped − undoped) showing the region above the valence band maximum of TiO_2. (b) Integrated area of the normalized photoelectron spectra below 3.0 eV (i.e., within the bandgap) of $Sn_xTi_{1-x}O_2$ solid solutions presented in Figure 6a.

of the valence band edge but by the tail of states extending into the bandgap. It is notable that the maximum in the intensity of structure above 3 eV is found for 4% Sn doping,whereas the maximum shift in the optical onset deduced from diffuse reflectance spectra is found a similar value (2−4% Sn doping, accounting for the magnitude of the error in the optical band gap measurement: see Figure 5e). A similar tailing of filled states above the VBM has been observed in SnO_2, and such states have been assigned to hybridized 5*s*−5*p* "lone pair" states associated with Sn(II) occupying surface sites. The reduction from Sn(IV) in the bulk to Sn(II) at the surface arises from oxygen deficiency at the surface.[28,54,55,57] If the cause of the states we observe above the VBM is oxygen deficiency, it is interesting to note that the characteristic band gap feature of oxygen deficient TiO_2 surfaces, the Ti(III) 3*d* peak with binding energy 0.7 eV,[55] was not observed in any of our samples. In accordance with the idea that there is a significant concentration of Sn(II) occupying surface sites it was found that the intensity of the Sn 3*d* core level peaks relative to that of Ti 2*p* was always higher than expected from the bulk doping level as is evident from data presented in table I. As has been discussed in detail elsewhere "lone pair" cations such as Sn(II) are more easily accommodated in surface sites than in bulk sites, thus providing a driving force for surface segregation.[57]

(56) Themlin, J. M.; Sporken, R.; Darville, J.; Caudano, R.; Gilles, J. M.; Johnson, R. L. *Phys. Rev. B* **1990**, *42*, 11914–11925.

(57) Cox, P. A.; Egdell, R. G.; Harding, C.; Patterson, W. R.; Tavener, P. J. *Surf. Sci.* **1982**, *123*, 179.

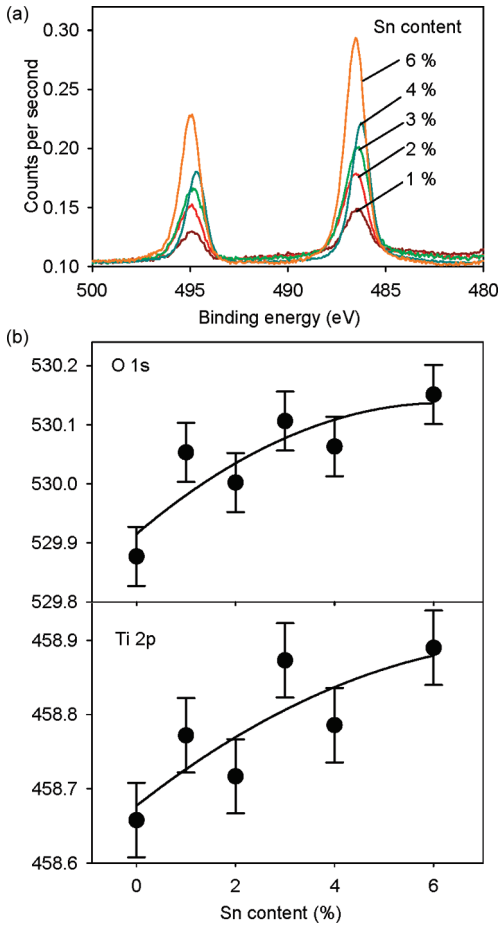

Figure 8. (a) Sn 3d core line photoelectron spectra of $Sn_xTi_{1-x}O_2$ solid solutions with the Sn contents indicted. (b) Variation in O 1s and Ti 2p core level binding energies in $Sn_xTi_{1-x}O_2$ solid solutions with increasing Sn content.

The Ti 2p and O 1s core lines show a shift to higher binding energy upon increasing Sn doping (Figure 8), while the Sn 3d core line shows no systematic variation in binding energy. If the CBM, and consequently the Fermi level, had decreased in energy, then a decrease in binding energy would be expected for the whole spectrum. However, the small change in CBM energy, estimated to be around 0.12 eV by Long et al.[33] might be masked by a larger core line chemical shift arising from final state effects. The averaged high frequency dielectric constant of SnO_2 ($\varepsilon_{av}(\infty) = 3.91$) is much smaller than that of TiO_2 ($\varepsilon_{av}(\infty) = 7.37$)[58] so that final state screening will be less pronounced in the former material as it is less polarizable. This will lead to a contribution to the chemical shift toward higher binding energy.

Conclusion

Phase pure $Sn_xTi_{1-x}O_2$ solid solutions have been prepared and characterized. Diffuse reflectance spectroscopy has clearly shown that Sn doping leads to narrowing of the band gap of TiO_2 in the concentration range investigated, with a minimum band gap of 2.995 eV at 2% Sn doping. In addition Sn doping leads to a broad tail of absorption that extends down to around 1.77 eV. XPS showed changes in the valence band density of states consistent with the substitution of Sn(IV) onto Ti(IV) sites, and additionally the presence new states above valence band maximum of undoped TiO_2 probably associated with segregated Sn(II) cations occupying surface sites. A small shift of the main valence band edge to low binding energy was also observed. The shift of the band edge is correlated with the shift in the main optical absorption onset, whereas the surface gap states produce a tail of weak absorption extending across the visible range. Systematic change in the CBM, which may also lead to band gap narrowing, was not observed but may have been masked by final state effects. Band bowing of the sort found here has been very extensively studied in III−V semiconductors.[59] However there has been less work on oxide systems and the extent of band bowing in oxide "alloys" such as $A_xZn_{1-x}O$ (A = Ca, Cd, Mg)[60] and $Si_xM_{1-x}O_2$ (M = Zr or Hf)[61] is expected to be rather small. Moreover no distinct minimum in the band gap is predicted by first principles calculations when the "wide gap" cation is substituted onto the host site. It has been argued that pronounced band bowing is only expected when the host and substituent ions have very different electronegativities.[62] The present finding of a distinct minimum in the band gap when Sn substitutes for Ti is somewhat surprising given that that the difference in electronegativity (on the Allred-Rochow scale) between Sn (1.72) and Ti (1.32) is less than between say Si (1.74) and Hf (1.23) or Zr (1.32). Further theoretical work is needed to explain the apparently anomalous behavior in $Sn_xTi_{1-x}O_2$ solid solutions.

Table I. Comparison of Bulk and Surface x Values Defined by Formula $Sn_xTi_{1-x}O_2$

bulk value of x[a]	surface value of x[b]
0.01	0.020
0.02	0.049
0.03	0.048
0.04	0.060
0.06	0.091

[a] Defined by stoichiometry of starting mixture. [b] From XPS measurements on Sn 3d and Ti 2p core lines after correction with atomic sensitivity factors.

Acknowledgment. The work in Oxford was supported in part by European Union grant NATAMA (NMP3-CT-2006-032583). The NCESS facility at Daresbury Laboratory is supported by EPSRC grant EP/E025722/1. F.E.O. is supported by Pembroke College Oxford and FUNDAYACUCHO (Caracas, Venezuela). M.H.H. is supported by MOE Brunei.

(58) Taverner, A. E.; Rayden, C.; Warren, S.; Gulino, A.; Cox, P. A.; Egdell, R. G. *Phys. Rev. B* **1995**, *51*, 6833–6837.
(59) Vurgaftman, I.; Meyer, J. R.; Ram-Mohan, L. R. *J. Appl. Phys.* **2001**, *89*, 5815–5875.
(60) Fan, X. F.; Sun, H. D.; Shen, Z. X.; Kuo, J. L.; Lu, Y. M. *J. Phys.: Condens. Matter* **2008**, 20.
(61) Nakhmedov, E. P.; Nadimi, E.; Bouhassoune, M.; Radehaus, C.; Wieczorek, K. *Phys. Rev. B* **2007**, 75.
(62) Tit, N.; Obaidat, I. M.; Alawadhi, H. *J. Comput. Theor. Nanosci.* **2009**, *6*, 1646–1653.